Supermetallic conductivity in bromine-intercalated graphite

S. Tongay,[1] J. Hwang,[1,2] D. B. Tanner,[1] H. K. Pal,[1] D. Maslov,[1] and A. F. Hebard[1,*]
[1]*Department of Physics, University of Florida, Gainesville, Florida 32611, USA*
[2]*Department of Physics, Pusan National University, Busan 609-735, Republic of Korea*
(Received 13 November 2009; published 16 March 2010)

Exposure of highly oriented pyrolytic graphite to bromine vapor gives rise to in-plane charge conductivities which increase monotonically with intercalation time toward values (for ~6 at % Br) that are significantly higher than Cu at temperatures down to 5 K. Magnetotransport, optical reflectivity and magnetic susceptibility measurements confirm that the Br dopes the graphene sheets with holes while simultaneously increasing the interplanar separation. The high-room-temperature mobility ($\sim 5\times 10^4$ $cm^2/V\cdot s$) and resistance anisotropy together with the reduced diamagnetic susceptibility of the intercalated samples suggests that the observed supermetallic conductivity derives from a parallel combination of weakly coupled hole-doped graphene sheets.

DOI: 10.1103/PhysRevB.81.115428 PACS number(s): 81.05.U−, 71.20.−b, 72.15.−v

I. INTRODUCTION

At the simplest level graphite can be thought of as an ordered stacking of weakly coupled graphene sheets. Delamination or deconstruction of graphite into isolated graphene sheets for experimental characterization by mechanical means[1] has nucleated intense experimental and theoretical investigation into the electronic properties of this two-dimensional (2D) carbon allotrope.[2] The presence of Dirac-like electronic excitations, an anomalous integer quantum Hall effect, and signature sensitivity to different types of disorder are but a few of the fascinating phenomena emerging from these studies. Bernal stacked graphite with an interplanar spacing $c=3.4$ Å manifests properties that are precursors to the unusual behaviors associated with graphene and few-layer graphene. For example the presence of Dirac fermions near the H point in the Brillouin zone has been detected by angle-resolved photoemission spectroscopy.[3]

Graphite intercalation compounds (GICs) have long been recognized as having unusual and sometimes surprising properties.[4] In this study we take the approach of using bromine (Br) intercalants to simultaneously dope and separate the planes of graphite and thereby begin an approach to the limit where the interplanar coupling is sufficiently weak to assure that the resulting in-plane conductivity can be considered as the parallel contribution of relatively independent doped graphene sheets. Since the band structure of graphite gives nearly equal numbers of electrons and holes, with a density on the order of 10^{-4} carriers per carbon atom,[5,6] a small charge transfer between the intercalate and the adjacent carbon planes can result in a significant increase in free carriers per carbon. We find that random site interplanar doping with bromine to concentrations ($\leq$6 at %) gives rise to a pronounced decrease of the in-plane resistivity ρ_{ab} to "supermetallic"[7] values that are significantly lower than Cu over the temperature range 300 K$>T>$1.7 K. Hall and x-ray photoelectron spectroscopy (XPS) measurements confirm that the Br dopant acts like an acceptor, thus hole doping the graphene planes. Optical reflectance measurements confirm the supermetallic in-plane conductivity and further reveal a doping-induced increase of mobility and carrier density. The diamagnetic susceptibility decreases toward zero as would be expected for isolated graphene sheets,[8] and there is no evidence of diamagnetic screening that might be associated with superconducting fluctuations. At $T=5$ K the inferred sheet resistance per graphene plane of less than 1 Ω is significantly lower than reported for isolated graphene sheets either biased by an adjoining gate[1] or doped with impurity atoms.[9]

II. EXPERIMENTAL

A. Sample preparation and characterization

The highly oriented pyrolytic graphite (HOPG) samples are cut from a single piece having 0.5° mosaic spread and typically have dimensions on the order of 1–5 mm. The samples are exposed to Br gas at room temperature in closed tubes for various intercalation times and then removed and measured in a four-contact arrangement using a LR700 17 Hz resistance bridge at temperatures and fields along the c axis in the ranges 5 K$<T<$300 K and −7 T$<B<$7 T, respectively. In highly anisotropic samples, precautions are needed to assure uniform current density between voltage leads.[10] We therefore used platelet (brick) shaped samples for the ρ_{ab} (ρ_c) measurements while taking care to assure uniformly contacted current leads for each case. Results for the resistivity of a given sample are reproducible to 1% and for twelve different samples cut from the same piece reproducible to 3%. After each measurement, additional intercalations could be made on the same sample. Weight uptake and volume increase, measured to an accuracy of ~3%, give a good measure of the correlation between Br concentration and doping time t_{Br}.

To characterize further the differences between pristine HOPG and the Br-doped samples, we also used x-ray diffraction (XRD), optical reflectance, Auger electron spectroscopy (AES), scanning electron microscopy (SEM), and x-ray photoelectron spectroscopy (XPS). SEM characterization did not detect any intercalation induced changes in surface morphology. The $\theta-2\theta$ XRD scans revealed only (00l) reflections that were shifted to lower angle (increased lattice spacing) with increased intercalation time and hence the concentration of Br between the graphene layers. This expansion is in

 ©2010 The American Physical Society

agreement with the observed swelling of the sample. There were no additional reflections indicating staging[4] or, equivalently, ordering of the Br intercalants. Optical reflectance measurements were made at 300 K using a Bruker 113v Fourier spectrometer over the range 40–5000 cm^{-1} (5–600 meV) and a Zeiss MPM 800 microspectrophotometer over 4000–40 000 cm^{-1} (0.5–5 eV). The low-frequency limit is set by the signal-to-noise and diffraction limitations of our small samples. Br LMM Auger peaks are observed to be located at 1396, 1442, and 1476 eV for Br exposure times $\geq$30 minutes. The samples were repeatedly cleaved and remeasured to probe the Br concentration at different depths of the sample; the peak heights for a given sample remained constant to within 5%. The Br concentrations extracted from the Auger measurements agreed well with the weight-uptake/volume-expansion measurements.

XPS spectra of bromine doped HOPG samples were measured with a 99% monochromatized Mg x-ray source with energies up to 1100 eV. Satellite peaks shifted by ~10 eV were barely visible. Elemental percentage analyses were found to be consistent with AES and weight uptake measurements. The C:1s electron binding energy measured relative to the Fermi level is observed to be at 284.5 eV for pristine and at 284.0 eV for the t_{Br}=70 min sample. At first sight, the reduction in the C:1s binding energy by 0.5 eV contradicts the acceptor nature of Br, i.e., the more positively charged carbon should, for fixed E_F, have a higher binding energy. However, similar trends/findings in donor (acceptor) type intercalants and associated increase (decrease) in C:1s binding energy have been reported in the literature for different compounds[11,12] and attributed to the change in E_F before and after intercalation. In brominated HOPG, E_F is negative and significantly larger in magnitude compared to pristine HOPG and the C:1s binding energy is thus measured with respect to the lower E_F of the hole-doped system. Accordingly, the increase in the C:1s binding energy is more than compensated for by the decrease in E_F, giving an overall decrease in the C:1s peak position as observed. The XPS method thus gives another way of estimating the change in Fermi level and implies a ~−0.5 eV change in E_F after hole doping to 6 at % Br.

B. Electrical transport measurements

Figure 1(a) shows the dependence of ρ_{ab} on Br intercalation time at T=300 K. Although the initial linear dependence is not understood, we note that after 70 min, ρ_{ab} appears to saturate at a value that is approximately a factor of five lower than the room-temperature value (1.7 $\mu\Omega$cm) of copper indicated by the horizontal dashed line. Our interpretation of how the carrier density N, the scattering time τ and the effective mass $m^\star$ are affected by Br intercalation is based on using the Drude model in which the conductivity σ of each contributing band is $\sigma=Ne^2\tau/m^\star=Ne\mu$, where the mobility $\mu=e\tau/m^\star$.

In Fig. 2 we show the evolution of the field (B) dependent transverse resistance ρ_{xy} for intercalation times t_{Br} ranging from t_{Br}=0 (pristine HOPG) to t_{Br}=70 min. The data for pristine HOPG are well fit by the expression for the two-band model,[6]

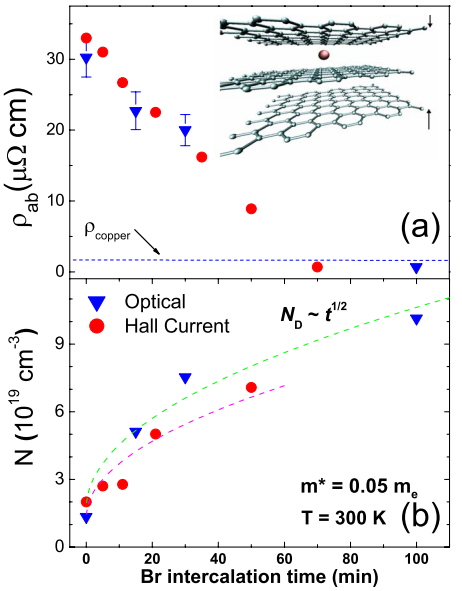

FIG. 1. (Color online) Plots of the room temperature in-plane resistivity ρ_{ab} (a) and carrier density N (b) as a function of Br intercalation time. The solid red circles (blue triangles) in both panels are inferred from transport/Hall (optical reflectance) measurements. After 100 min ρ_{ab} is reduced by a factor of 100 below its starting value to a resistivity that is a factor of five below that of copper (horizontal dashed line).

$$\frac{\rho_{xy}(B)}{e\rho_{xx}(0)^2}=\frac{(-n_e\mu_e^2+n_h\mu_h^2)B+\mu_e^2\mu_h^2(n_h-n_e)B^3}{1+e^2\rho_{xx}(0)^2\mu_e^2\mu_h^2(n_h-n_e)^2B^2}, \quad (1)$$

where $\rho_{xx}(0)$ is the B=0 in-plane resistivity and the subscripts e and h refer respectively to the electron and hole bands. The obtained fitting parameters are $n_h=2.0(1)\times10^{19}$ cm^{-3}, $n_e=1.6(1)\times10^{19}$ cm^{-3}, μ_h =4700(100) $cm^2/V\cdot s$, and μ_e=6800(100) $cm^2/V\cdot s$ showing that our pristine HOPG is slightly hole doped with similar mobilities in each band. In graphite, Eq. (1) is applicable for $\mu B\gtrsim1$, when $\rho_{xx}(B)$ is quadratic in B.[13] At T=300 K,

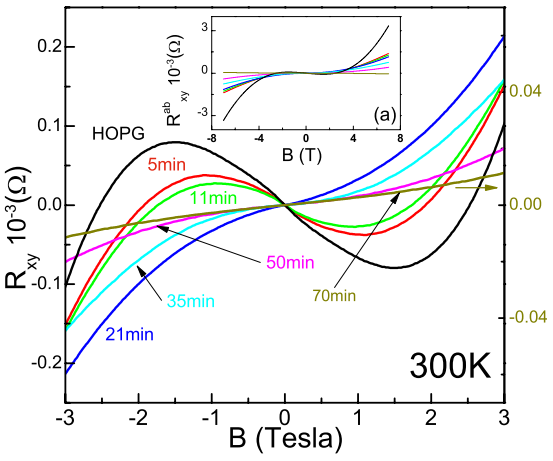

FIG. 2. (Color online) Transverse resistance ρ_{xy} as a function of perpendicular magnetic field B for the indicated intercalation times. The inset shows the same data over a larger field range.

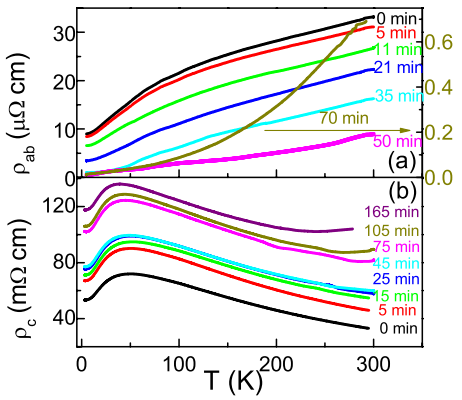

FIG. 3. (Color online) Temperature dependence of (a) ρ_{ab} and (b) ρ_c at the indicated intercalation times. The right hand axis of panel (a) is an expanded scale for the $t_{\mathrm{Br}}=70$ min curve

$\mu B=1$ corresponds to $B=0.3$ T in pristine graphite, so Eq. (1) describes most of the field range presented in Fig. 2. With increasing t_{Br}, the quadratic dependence of $\rho_{xx}(B)$ occurs over a decreasing field range, thus restricting the range of validity of Eq. (1). Constrained by this requirement, we extract a square-root dependence of N on t_{Br} shown in Fig. 1(b). As seen in Fig. 2, the low-field slope, which is positive for $t_{\mathrm{Br}} \geq 20$ min. decreases with increasing Br concentration and becomes linear for the highest t_{Br}, thus indicating that Br is hole doping the graphene sheets with a carrier density $N=n_h$ dominated by holes.

The temperature-dependent resistivity data of panels (a) and (b) of Fig. 3 show that the resistivity scales for ρ_{ab} (ρ_c) decrease (increase) as T is reduced from 300 K to 5 K. The positive curvature for samples with $t_{\mathrm{Br}} \geq 70$ min. is consistent with the notion that the doping is sufficient to guarantee $E_F \gg k_B T$ in contrast to pristine HOPG and the lightly doped samples where $E_F \sim 300$ K and significant variation of N with T leads to a negative curvature of $\rho_{ab}(T)$. The ratio $\rho_{ab}(300\ \mathrm{K})/\rho_{ab}(5\ \mathrm{K})=47$ for the sample with $t_{\mathrm{Br}}=70$ min. is higher by more than a factor of 10 than the same ratio (4.0) for pristine HOPG. In contrast to ρ_{ab}, ρ_c increases with increasing t_{Br} due to the presence of Br intercalants acting like a negative pressure pushing the planes apart [see schematic inset of Fig. 1(a)], thereby resulting in decreased interplanar tunneling. With the application of positive pressure the interplanar spacing decreases and there is a corresponding decrease in ρ_c.[14] The hole doping of the planes (decreasing ρ_{ab}) concomitant with an increasing interplanar spacing (increasing ρ_c) leads to an anisotropy ratio ρ_c/ρ_{ab} at 5 K approaching 10^7, a factor of 1000 greater than measured for pristine HOPG at the same temperature.

C. Optical measurements

With increasing t_{Br} the far infrared and midinfrared reflectance increase dramatically as shown in Fig. 4(a). This increase in reflectance implies an associated increase in optical conductivity which is borne out by a Kramers–Kronig analysis.[15] We used a Drude extrapolation at low frequencies and a power-law behavior at high frequencies, with the results shown in Fig. 4(b). Note that the optical conductivity

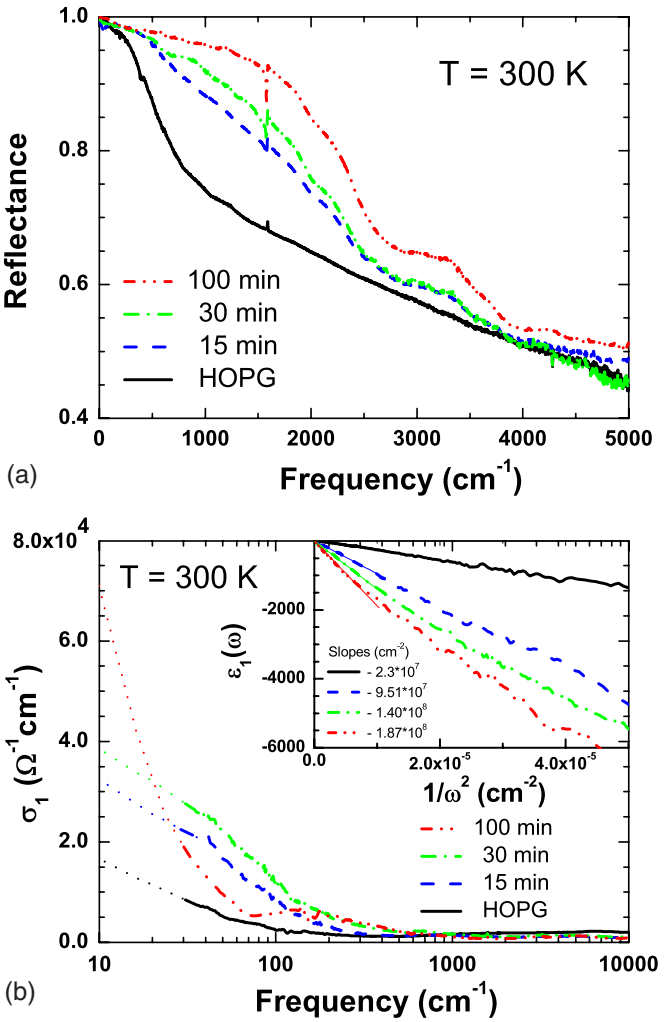

FIG. 4. (Color online) Infrared reflectance (a) and optical conductivity, $\sigma_1(\omega)$, (b) at indicated intercalation times t_{Br}. Data below 35 cm^{-1} in panel (b) are from the Drude–Lorentz fit to the reflectance. Inset: Real part of the dielectric function versus $1/\omega^2$. The slope, proportional to the plasma frequency squared, is a measure of the total carrier density.

curves include frequencies (dashed lines) where we used the extrapolation; the good agreement with the dc conductivity in Fig. 1(a) and the good fits to the reflectance provide confidence that the behavior is as shown. As the doping proceeds, the low-frequency conductivity increases and the spectral weight (the area under the curve) increases significantly [Fig. 4(b)]. The full width of this Drude-like peak represents the carrier scattering rate τ^{-1} which at the highest doping is decreased by a factor of five relative to the pristine sample.

We also note in the raw reflectance data of Fig. 4(a) the appearance of a phonon mode around 1580 cm^{-1}. This mode, which appears to strengthen and develop a Fano lineshape with Br intercalation, can barely be seen as a small feature above the line in the conductivity spectra of Fig. 4(b). To show this feature in more detail, we have magnified the appropriate region by a factor of 1000 as shown in Fig. 5. The weak optical phonon near 1588 cm^{-1} increases in strength by nearly a factor of four and red shifts by 3 cm^{-1}.

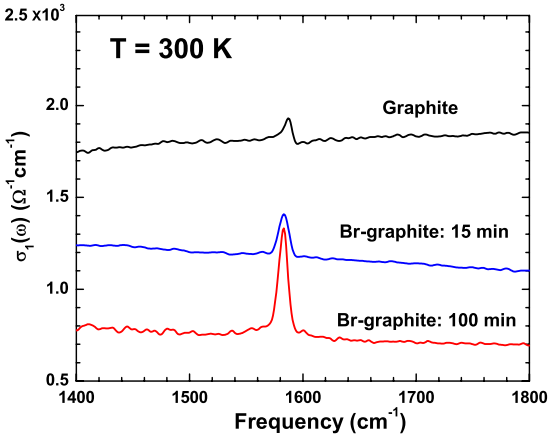

FIG. 5. (Color online) Optical conductivity of graphite and Br-doped graphite in the region of the 1588 cm^{-1} phonon corresponding to the intercalation times t_{Br} (top to bottom) indicated in the legend.

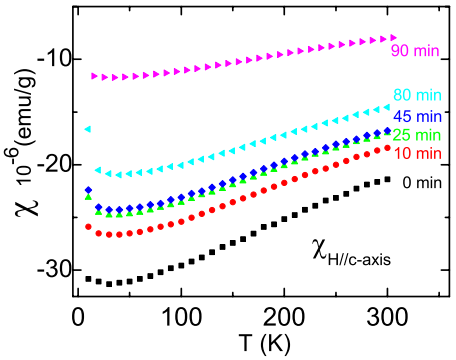

FIG. 6. (Color online) Temperature dependence of magnetic susceptibility χ_c at the indicated intercalation times.

These trends are consistent with prior results,[16] which show that intercalation changes the lineshape, lowers the frequency, and also leads to higher oscillator strength of this mode. Metallic behavior thus persists out to these energies in the strongly intercalated samples.

From the sum rule on the optical conductivity, we can relate the low-energy spectral weight to the carrier density. The spectral weight also affects the real part of the dielectric function, $\epsilon_1(\omega)$, which for free carriers follows $\epsilon_1(\omega)=1-\omega_p^2/\omega^2$, where $\omega_p^2=4\pi Ne^2/m^\star$ is the plasma frequency. The inset of Fig. 4(b) shows $\epsilon_1(\omega)$ plotted vs $1/\omega^2$; the slopes of these plots give the carrier density, which is seen to increase by more than a factor of eight with increasing t_{Br}. That the curves are straight lines implies strongly that a free-carrier (metallic) picture of the low-energy electrodynamics is an accurate view of the intercalated graphite. The dc resistivities inferred from the Drude fit to the infrared reflectance measurements are shown as blue triangles in Fig. 1(a). Because the reflectance measurements are made without placing electrical contacts on the sample, the inferred dc conductivities of Fig. 4(b) give independent confirmation of the supermetallic conductivity inferred from transport measurements.

D. Magnetization measurements

Figure 6 shows that the temperature-dependent dc diamagnetic susceptibility χ (field parallel to c axis) decreases with increasing t_{Br}. Our room-temperature value for pristine graphite, $\chi=-21.3\times10^{-6}$ emu/g, is in good agreement with previous experiments;[5,8] the susceptibility decreases by a factor of three for $t_{Br}=90$ min. This decrease in χ with increased hole doping of the graphene planes is qualitatively understood by realizing that as the Fermi energy moves away from the neutrality point ($n_h=n_e$) of pristine graphite, the cyclotron mass $m_c^\star$ increases and $\chi\propto1/m_c^\star$ decreases, approaching the limit of exponentially weak diamagnetism for single-plane Dirac fermions. Importantly, there is no signature of superconductivity, which, if associated with the giant conductivity, would become manifest as an *increase* in diamagnetism at some characteristic temperature.

III. DISCUSSION

Graphite intercalation compounds in the dilute limit are well known to exhibit enhancements of room-temperature conductivity which, with increasing intercalant concentration, saturate to modest values ~10 times the pristine value.[17] The surprising and unexpected result presented here is that for uniformly dispersed nonstaged Br dopants at relatively low concentrations near 5–6 at%, the conductivity can justifiably be referred to as "supermetallic." To make comparisons to single-layer graphene, we convert our ρ_{ab} measurements to resistance per square R_g of each carbon plane and see that R_g near 1000 Ω for HOPG at 300 K decreases to less than 0.5 Ω at 5 K for intercalated samples with $t_{Br}=70$ min. To our knowledge, there are no reports of such a low R_g for graphene.

The experimental results raise many questions, e.g., since doping introduces disorder, why does the conductivity increase? At high-doping level, most of the carriers (holes) come from negatively charged acceptors, so we have a system, in which the number of carriers is approximately equal to the number of scattering centers. On the other hand, since the Fermi energy shifts downward and increases with doping, the scattering cross-section decreases, so we have two competing effects. Assuming for a moment that the scattering cross-section is of the 2D classical Rutherford form $A_R\sim e^2/E_F$, that E_F obeys the 2D scaling $E_F\propto n_a$, where $n_a=n_hc$ is the number density of acceptors per layer, and estimating the mean free path as $\ell=1/n_aA_R$, we arrive at a simple result for the parameter $k_F\ell$, which characterizes purity of a material: $k_F\ell\sim1/r_s$, where r_s is the average inter-carrier distance measured in Bohr radii. Already in pristine graphite, $r_s\sim1$ (Ref. 18) and it decreases further with doping, so this simple model predicts that the material becomes "cleaner" with doping, concomitant with an increase in the 2D conductivity, which is proportional to $k_F\ell$.

In reality, this simple picture is modified significantly due to effects of screening. To see this in more detail, we consider the screening mechanism in doped graphite. In pristine graphite, the Fermi energy $E_F\approx225$ meV is on the order of

the hopping energy between the next-to-nearest graphene layers, γ_2. Upon doping, the Fermi energy increases. We consider two limiting cases: (i) $\gamma_2 \ll E_F \ll \gamma_1$ and (ii) $\gamma_1 \ll E_F \ll \gamma_0$, where $\gamma_1 \approx 0.3$ eV is the nearest-layer hopping and $\gamma_0 \approx 3.2$ eV is the nearest-neighbor hopping in the graphene plane. In the first case, graphite is the "bilayer regime":[18] the energy spectrum of holes is approximately $\varepsilon_{\mathbf{k}} = -\hbar^2 k_\parallel^2 / 2m_\parallel(k_z)$, where $m_\parallel(k_z) = \bar{m}_\parallel \cos(k_z c/2)$ is the k_z dependent in-plane mass with $\bar{m}_\parallel \equiv \gamma_1 / v_0^2$, $v_0 \approx 10^8$ cm/s is the Dirac velocity, and $c \approx 6.8$ Å is the c axis lattice constant. The density of states (per spin and per K point of the graphite Brillouin zone) in this regime $\nu = \gamma_1 / \hbar^2 \pi^2 v_0^2 c$ does not depend on the electron energy. In the second case, graphite is in the graphene regime: the spectrum is Dirac-like $\varepsilon_{\mathbf{k}} = -\hbar v_0 k_\parallel$ and the density of states $\nu = \varepsilon / 2\pi^2 \hbar^2 v_0^2 c$ increases linearly with energy ε. In the Thomas–Fermi model, the square of the screening wave vector is $\kappa^2 = 16\pi e^2 \nu$. Although κ increases with E_F, it still remains much smaller than the reciprocal lattice constant for not too high dopings. Indeed, it is easy to see that $\kappa^2 c^2 \sim (c/a_B)(E_F/\gamma_1)$ in the graphene regime, where $a_B = \epsilon_0 \hbar^2 / e^2 \bar{m}_\parallel \approx 50$ Å for the background dielectric constant $\epsilon_0 = 5$.[19] Therefore, $\kappa^2 c^2 \lesssim 1$ for $E_F \lesssim 10\gamma_1 \approx \gamma_0$. Accordingly, in both the bilayer and graphene regimes screening is not sensitive to details of the spectrum, all of which are incorporated into the density of states. In the continuum limit, with the screening radius large compared to the lattice constant, the screened potential is isotropic.

The above arguments allow us to model the potential of a single charged acceptor by a simple Thomas–Fermi form,

$$V(q) = -\frac{4\pi e^2}{q_\parallel^2 + q_z^2 + \kappa^2}, \tag{2}$$

where $\hbar q_\parallel$ and $\hbar q_z$ are the in-plane and c-axis momentum transfers of charge carriers. The scattering time can be then obtained from the Fermi Golden Rule

$$\frac{1}{\tau} = \frac{2\pi}{\hbar} n_a \int \frac{d^2 q_\parallel}{(2\pi)^2} \int \frac{dq_z}{2\pi} V^2(q) \delta(\varepsilon_{\mathbf{k}_\parallel + \mathbf{q}_\parallel, k_z + q_z} - \varepsilon_{\mathbf{k}_\parallel, k_z}). \tag{3}$$

Another simplification comes from the fact that $q_\parallel$ is bounded by twice the in-plane radius of the Fermi surface $k_{F\parallel} \sim \sqrt{n_a} c$, which is smaller than κ for not too high dopings. This implies that one can neglect $q_\parallel$ in Eq. (2). On the other hand, as typical $q_z \sim \kappa \ll 1/c$, one can neglect q_z in the energies entering the δ function in Eq. (3). The integral over q_z can be then performed independently of that over $\mathbf{q}_\parallel$ and yields an effective coupling constant for in-plane scattering $\bar{V} = \int dq_z V^2(q)/2\pi = 4\pi^2 e^4 / \kappa^3$. In terms of $\bar{V}$, the scattering rate can be written as

$$\frac{1}{\tau} = \frac{2\pi}{\hbar} n_a \bar{V} \nu_{2D}, \tag{4}$$

where

$$\nu_{2D} = \int \frac{d^2 q_\parallel}{(2\pi)^2} \delta(\varepsilon_{\mathbf{k}_\parallel + \mathbf{q}_\parallel, k_z} - \varepsilon_{\mathbf{k}_\parallel, k_z}), \tag{5}$$

is the effective density of states per graphene layer. Accordingly, charged acceptors act effectively as short-range scatterers, which affect only the in-plane motion of electrons. *A posteriori*, this explains why we ignored the difference between the total and transport scattering times. In the bilayer regime, $\nu_{2D} = m_\parallel(k_z)/2\pi\hbar^2$, while in the graphene regime $\nu_{2D} = \varepsilon / \hbar^2 v_0^2$. In both cases, $\nu_{2D} \sim \nu c$. Therefore, one can write down the following estimate for $1/\tau$:

$$\frac{1}{\tau} \sim \frac{e^2}{\hbar} \frac{n_a c}{\kappa}.$$

In the bilayer regime, κ does not depend on n_a and, therefore, $1/\tau$ increases linearly with doping. In the graphene regime, κ does increase with doping (so that the effective scattering cross-section decreases) but only weakly—as $\nu^{1/2} \propto E_F^{1/2} \propto n_a^{1/4}$—and $1/\tau$ still increases with n_a (as $n_a^{3/4}$). We see, therefore, that the observed nonmonotonic dependence of $1/\tau$ on doping shown in Fig. 7 cannot be explained within a model of scattering from randomly placed charged acceptors.

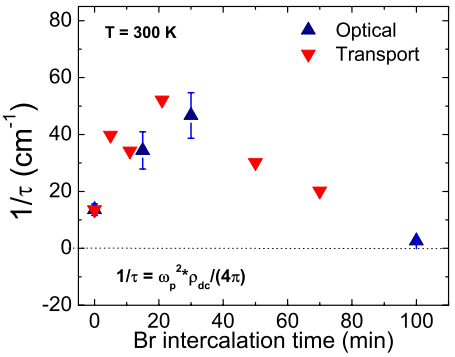

FIG. 7. (Color online) Plot of scattering rates determined from optical (blue triangles) and transport (red triangles) shows nonmonotonic dependence on bromine intercalation times.

A decrease of $1/\tau$ with doping may be attributed to partial ordering of Br ions: the absence of three-dimensional order (staging) does not preclude formation of a laminar structure, in which there is no correlation between ordered layers of the intercalant.[20] Scattering of charge carriers by such layers will be suppressed due to miniband formation (if the Fermi energy lies outside the forbidden gaps) in exactly the same way (partial) ordering of donors in modulation-doped semiconductor heterostructures is believed to be responsible for extremely high-carrier mobilities in such structures.[21] At the highest doping level achieved in this study (bulk number density $n = 10^{20}$ cm^{-3} or sheet density per graphene layer $nc/2 = 3.4 \times 10^{12}$ cm^{-2}), the average distance between Br intercalants is 30 Å. For $\epsilon_0 = 5$, the Coulomb energy at this distance is about 0.1 eV, which is about 4 times larger than the thermal energy at room temperature. Theoretical and experimental studies of 2D classical Wigner crystals on structureless (liquid) substrates show that the Coulomb energy exceeds the thermal energy at the melting temperature by a factor of 127.[22] According to this criterion, a Wigner crystal is not expected to be stable above 10 K in our case. Screening by mobile carriers should lead to a further reduction of the melting temperature. Nevertheless, the 2D order can be stabilized due to the presence of crystalline substrate

(graphene sheets). Also, a fully developed 2D order may not be needed–long-range correlations in the positions of Br ions may be enough to reduce their effect on the mobility of free carriers. A detailed analysis of this question requires separate experimental and theoretical studies which are outside the scope of this paper.

The mobility of Br-intercalated HOPG at room temperature, confirmed by optical measurements, is 50 000 $cm^2/V \cdot sec$, a factor of 5 higher than pristine HOPG. From transport data at 5 K we find $\mu_h \sim 10^6$ $cm^2/V \cdot s$ but consider this with some reservations in the absence of confirming optical data. Although we have not reached the limit where the interplanar coupling is sufficiently low to consider our intercalated graphite as an ordered stack of isolated graphene sheets each of which is dominated by Dirac fermions, we believe our results illustrate the emergence of intriguing phenomenology at the graphite/graphene boundary accessed by intercalation.

ACKNOWLEDGMENTS

We thank D. Arenas, H.-P. Cheng, V. Craciun, J. E. Fischer, E. Lambers, and B. Shklovskii for useful discussions. This research was supported by the NSF and DOE under Grants No. DMR-0704240(AFH) and No. DE-FG02-02ER45984(DBT).

*Corresponding author; afh@phys.ufl.edu

[1] K. S. Novoselov, A. K. Geim, S. V. Morozov, D. Jiang, Y. Zhang, S. V. Dubonos, I. V. Grigorieva, and A. A. Firsov, Science **306**, 666 (2004).

[2] A. H. Castro Neto, F. Guinea, N. M. R. Peres, K. S. Novoselov, and A. K. Geim, Rev. Mod. Phys. **81**, 109 (2009).

[3] S. Y. Zhou, G. H. Gweon, J. Graf, A. V. Fedorov, C. D. Spataru, R. D. Diehl, Y. Kopelevich, D. H. Lee, S. G. Louie, and A. Lanzara, Nat. Phys. **2**, 595 (2006).

[4] M. S. Dresselhaus and G. Dresselhaus, Adv. Phys. **30**, 139 (1981).

[5] N. B. Brandt, S. M. Chudinov, and G. Ya, *Ponomarev, Semimetals 1: Graphite and its Compounds* (North-Holland, Amsterdam, 1988).

[6] X. Du, S. W. Tsai, D. L. Maslov, and A. F. Hebard, Phys. Rev. Lett. **94**, 166601 (2005).

[7] The adjective "supermetallic" has been used in early work to describe staged GICs which exhibit a room-temperature resistivity several times lower than copper, N. B. Brandt, S. G. Ionov, S. V. Kuvshinnikov, V. A. Mikhanov, and V. V. Avdeef, JETP Lett. **34**, 243 (1981).

[8] J. W. McClure, Phys. Rev. **119**, 606 (1960).

[9] F. Schedin, A. K. Geim, S. V. Morozov, E. W. Hill, P. Blake, M. I. Katsnelson, and K. S. Novoselov, Nature Mater. **6**, 652 (2007).

[10] G. M. T. Foley, C. Zeller, E. R. Falardeau, and F. L. Vogel, Solid State Commun. **24**, 371 (1977).

[11] G. K. Wertheim, P. Vanattekum, and S. Basu, Solid State Commun. **33**, 1127 (1980).

[12] Z. Yan, Z. Zhuxia, L. Tianbao, L. Xuguanga, and X. Bingshe, Spectrochim. Acta, Part A **70**, 1060 (2008).

[13] H. K. Pal and D. L. Maslov (unpublished).

[14] C. Uher, R. L. Hockey, and E. Ben-Jacob, Phys. Rev. B **35**, 4483 (1987).

[15] F. Wooten, *Optical Properties of Solids* (Academic Press, San Diego, 1972).

[16] M. S. Dresselhaus and G. Dresselhaus, Adv. Phys. **51**, 1 (2002); S. Y. Leung, C. Underhill, G. Dresselhaus, and M. S. Dresselhaus, Solid State Commun. **33**, 285 (1980); Alain Moissette, Andre Burneau, Jean Dubessy, Herve Fuzellier, and Michele Lelaurain, Carbon **33**, 1223 (1995).

[17] M. S. Dresselhaus, G. Dresselhaus, and J. E. Fischer, Phys. Rev. B **15**, 3180 (1977).

[18] D. B. Gutman, S. Tongay, H. K. Pal, D. L. Maslov, and A. F. Hebard, Phys. Rev. B **80**, 045418 (2009).

[19] H. Venghaus, Phys. Status Solidi B **81**, 221 (1977).

[20] B. I. Shklovskii (private communication).

[21] A. L. Efros, F. G. Pikus, and G. G. Samsonidze, Phys. Rev. B **41**, 8295 (1990).

[22] See, e.g., S. T. Chui and K. Esfarjani, Phys. Rev. B **44**, 11498 (1991) and references therein.